

Supplementary Material

Supplementary Figures

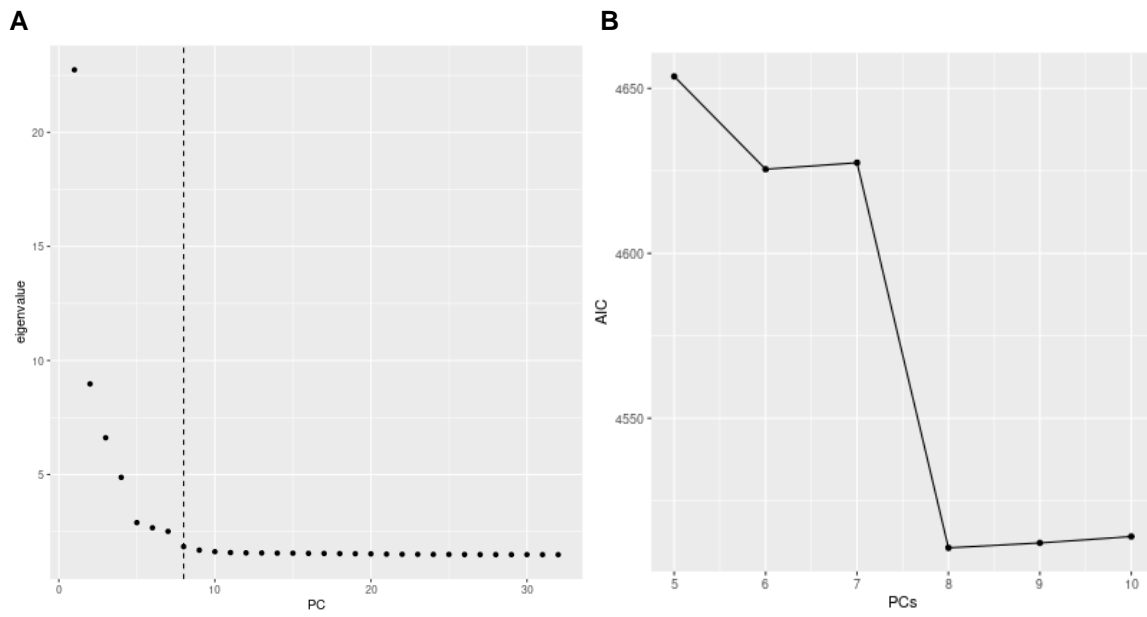


Figure S1. Selection of Principal Components (PCs) of ancestry to include as covariates in the GWAS. A) Scree Plot showing the eigenvalues of principal components 1 to 32. B) Plot showing the Akaike Information Criterion (AIC) for null models fitted with a varying numbers of principal components.

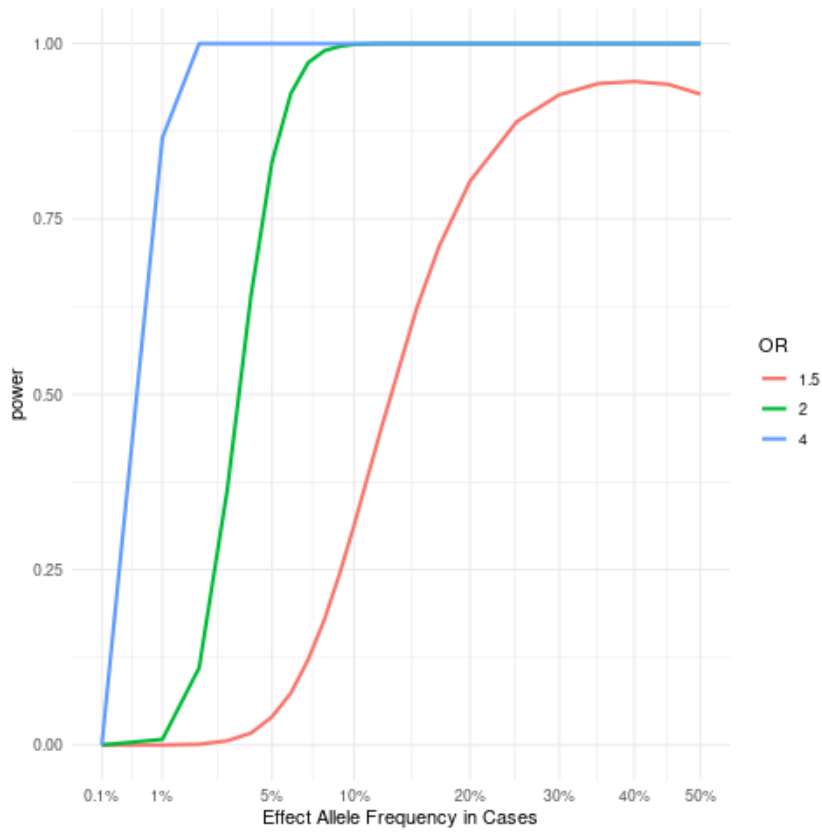


Figure S2. Plot of statistical power (y axis) vs effect allele frequencies (x axis), for detecting genome-wide significant associations in the present study (1067 cases vs 3799 controls), for varying ORs (colored lines). A population prevalence of MacTel of 0.45%, and an additive genetic model is assumed.

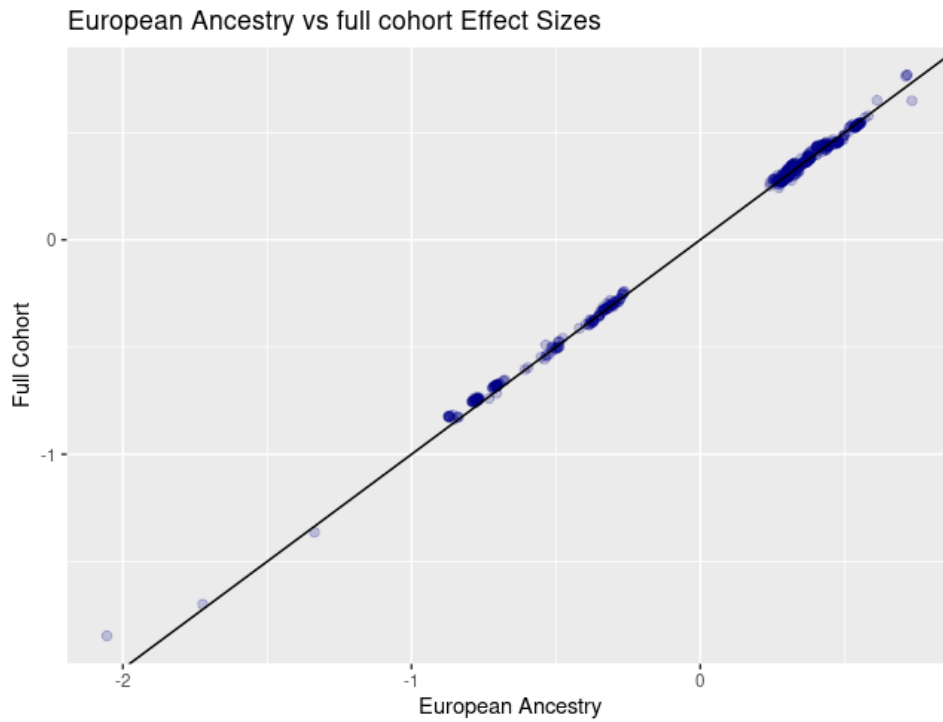
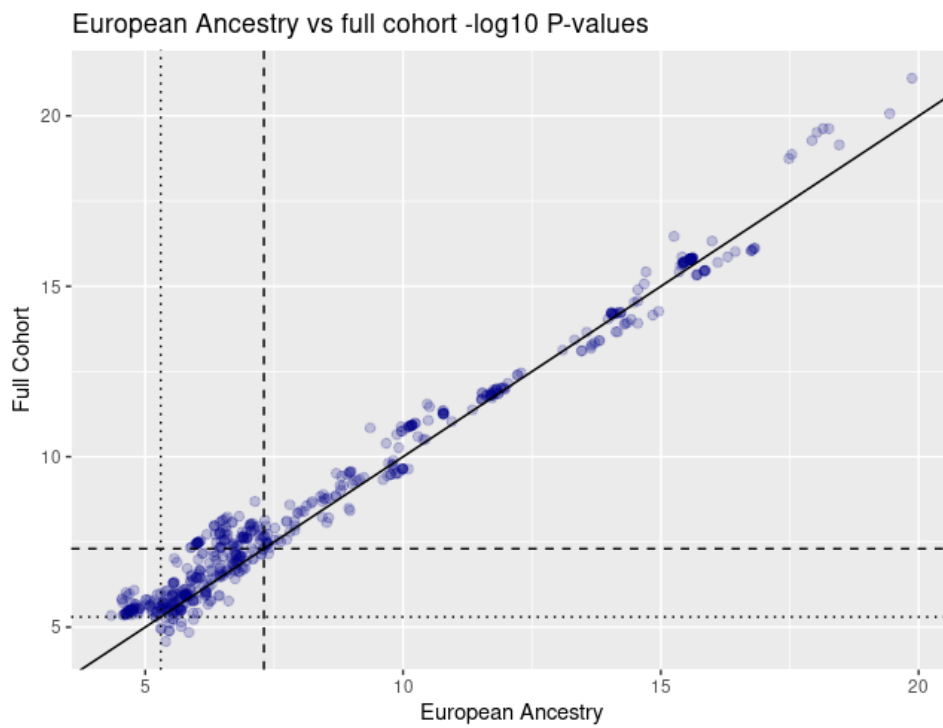
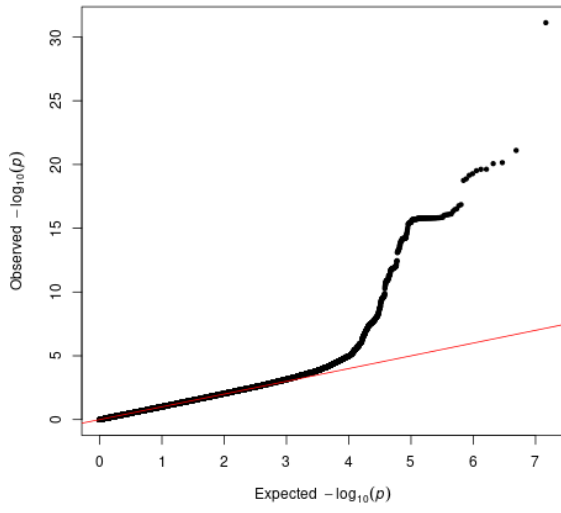
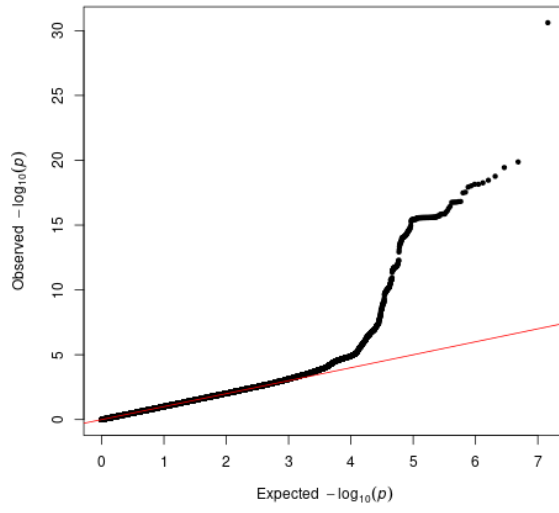
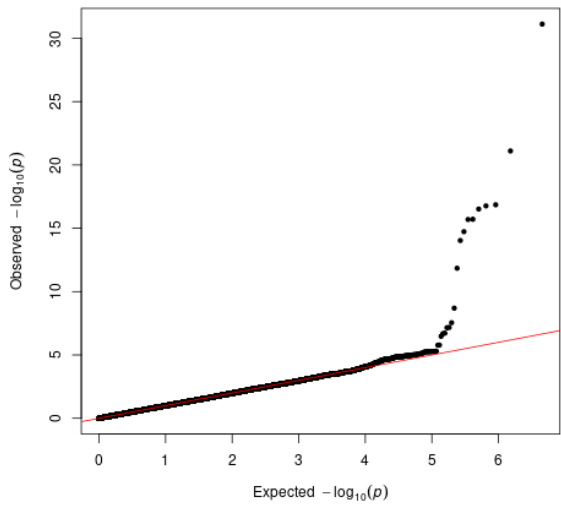
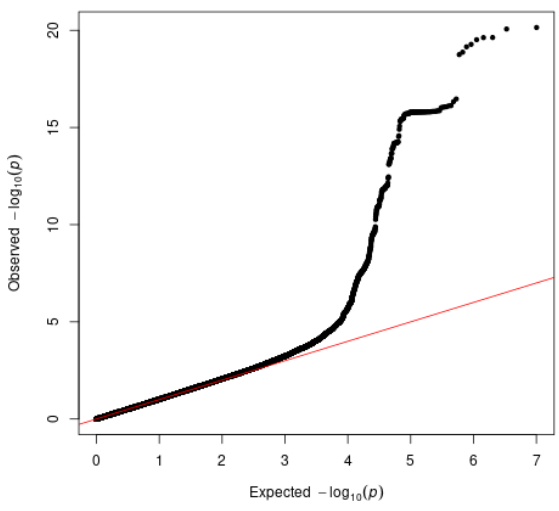
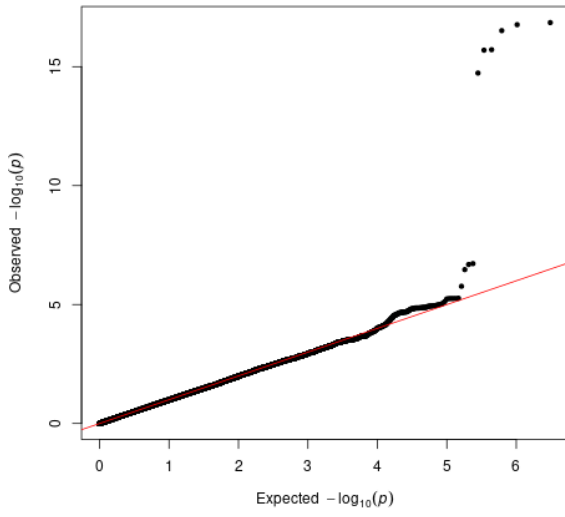
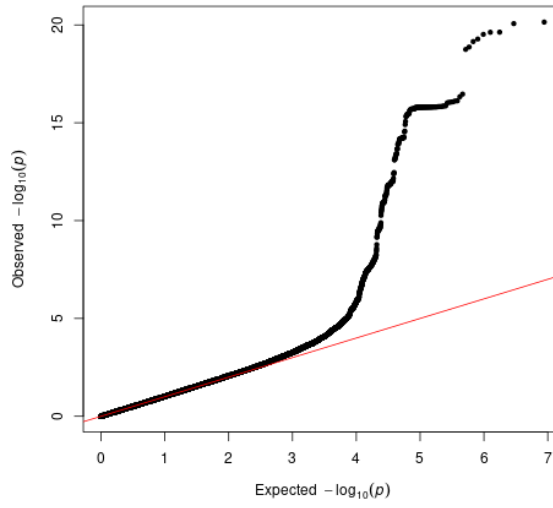
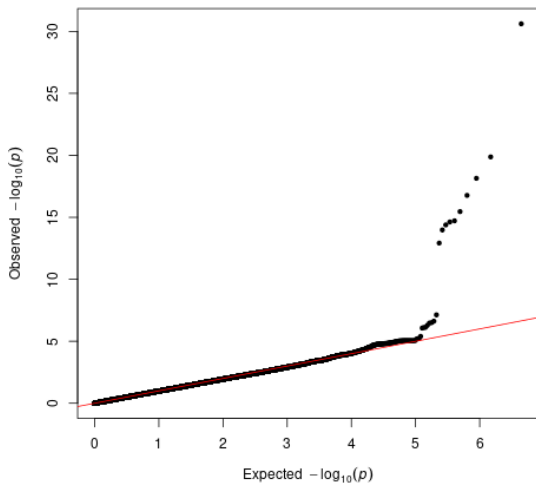
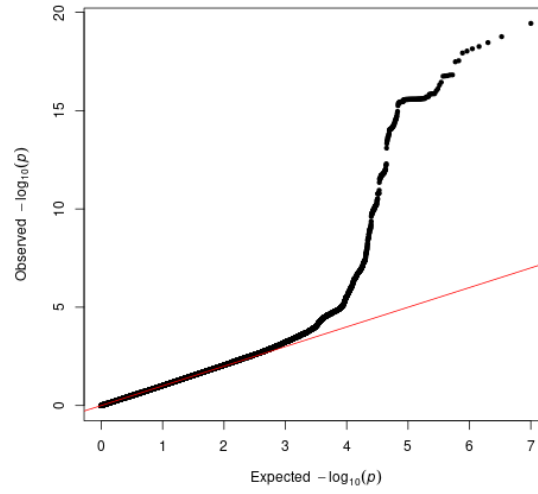
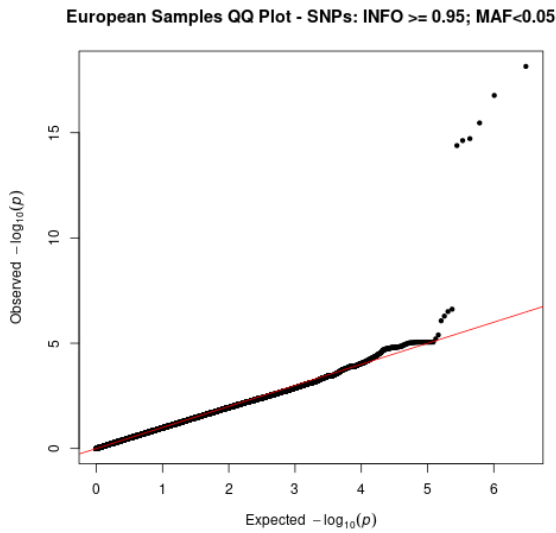
A**B**

Figure S3. Comparison of A. effect sizes and B. P-values, from the full cohort analysis, and European Ancestry analysis. Shown are all SNPs meeting suggestive significance ($P < 5E-6$) in either analysis.

A**All Ancestries QQ Plot****B****European Samples QQ Plot****C****All Ancestries QQ Plot - SNPs: INFO ≥ 0.9 ; MAF < 0.05** **D****All Ancestries QQ Plot - SNPs: INFO ≥ 0.9 ; MAF ≥ 0.05** 

EAll Ancestries QQ Plot - SNPs: INFO ≥ 0.95 ; MAF < 0.05 **F**All Ancestries QQ Plot - SNPs: INFO ≥ 0.95 ; MAF ≥ 0.05 **G**European Samples QQ Plot - SNPs: INFO ≥ 0.9 ; MAF < 0.05 **H**European Samples QQ Plot - SNPs: INFO ≥ 0.9 ; MAF ≥ 0.05 

I



J

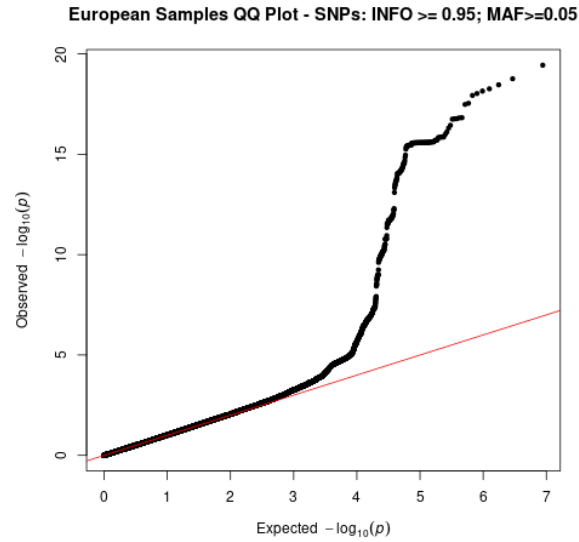
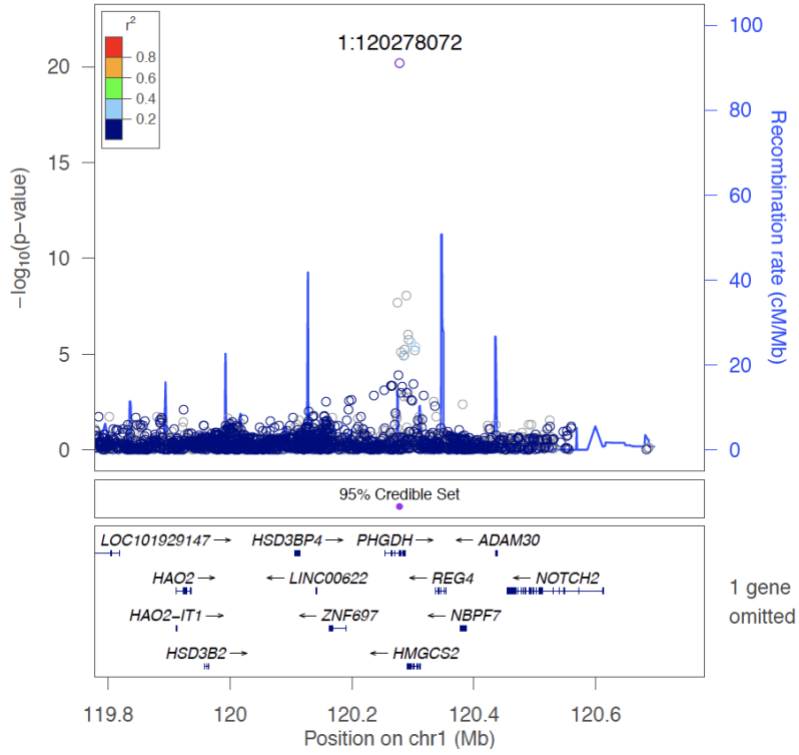
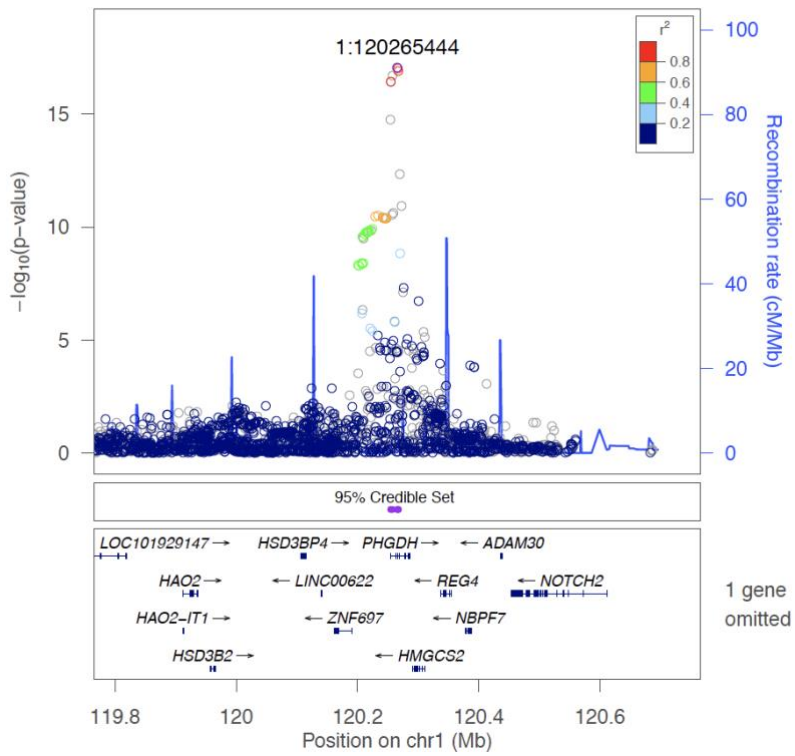
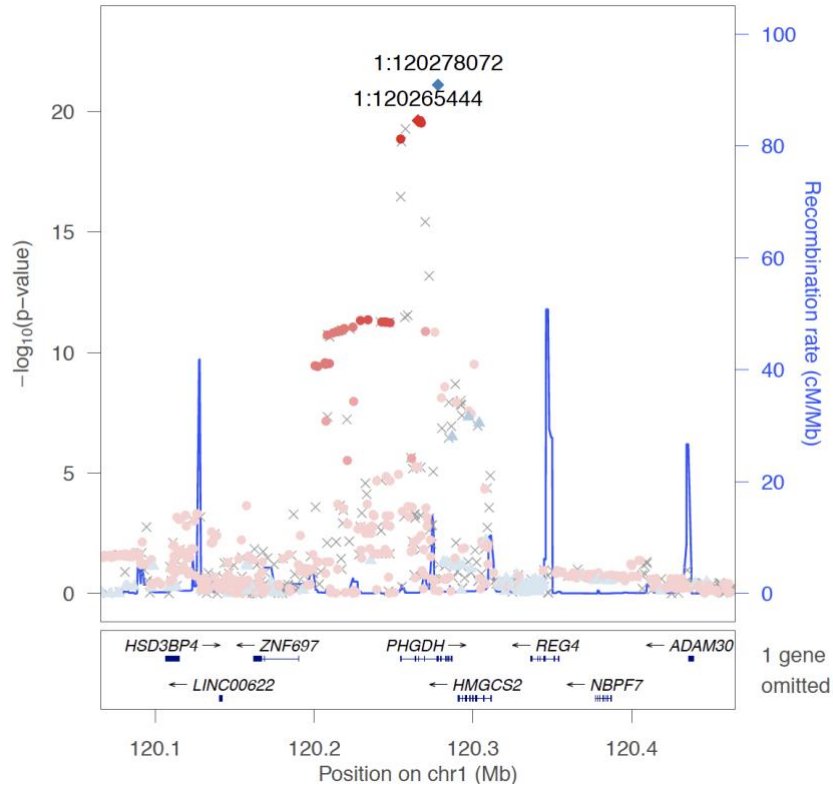
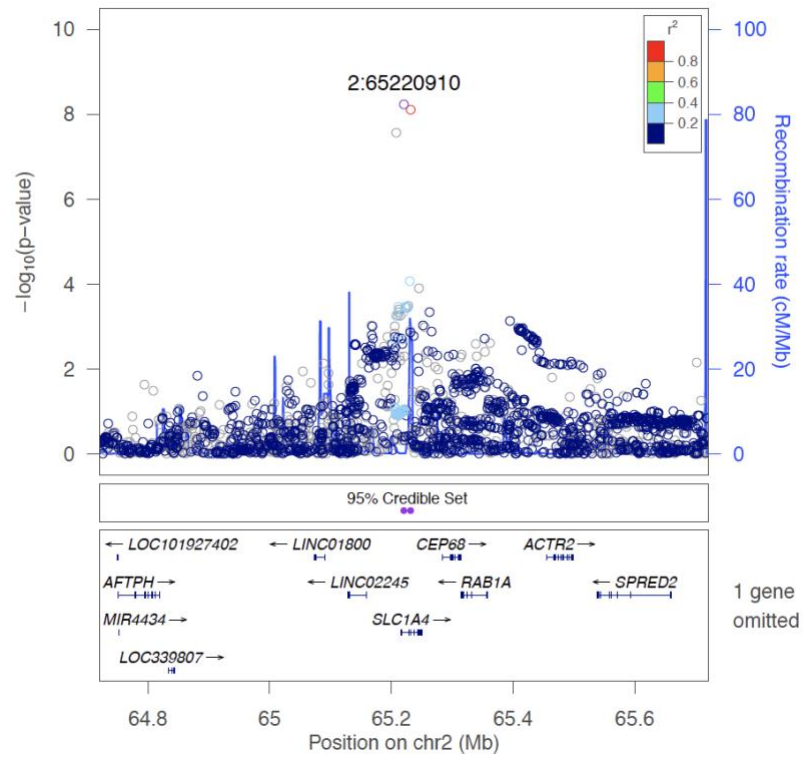
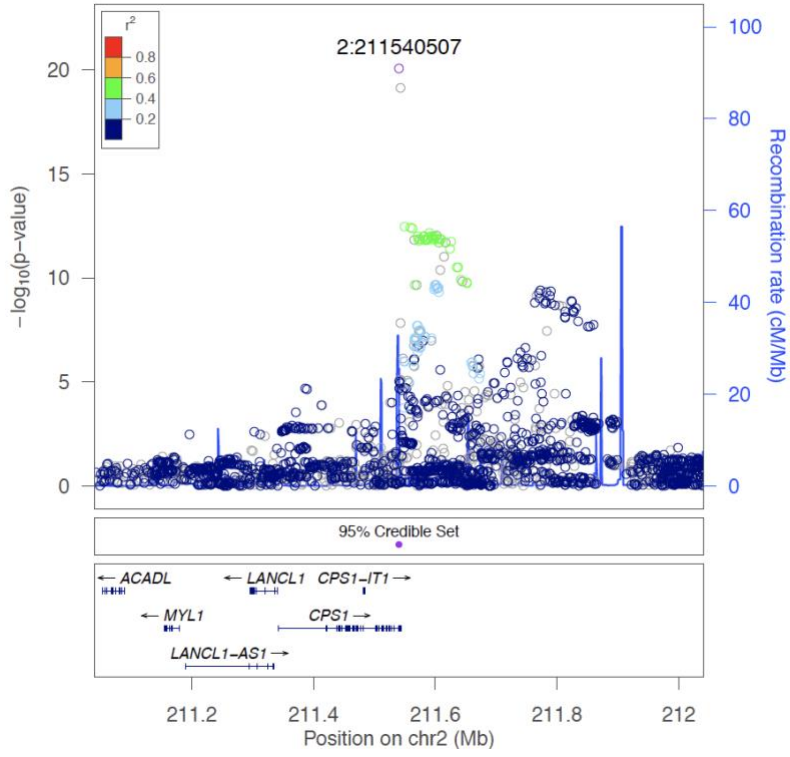
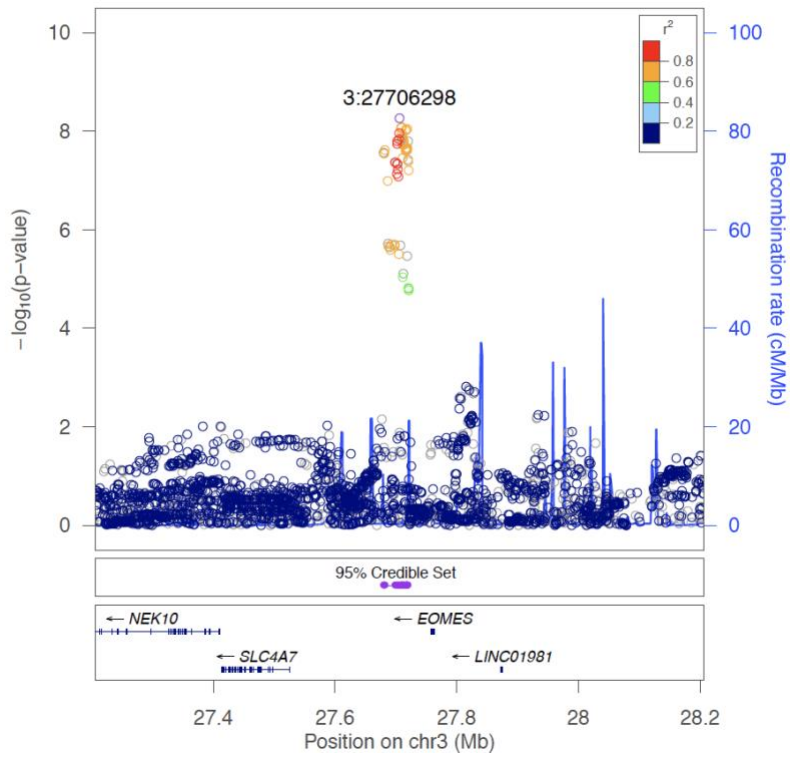


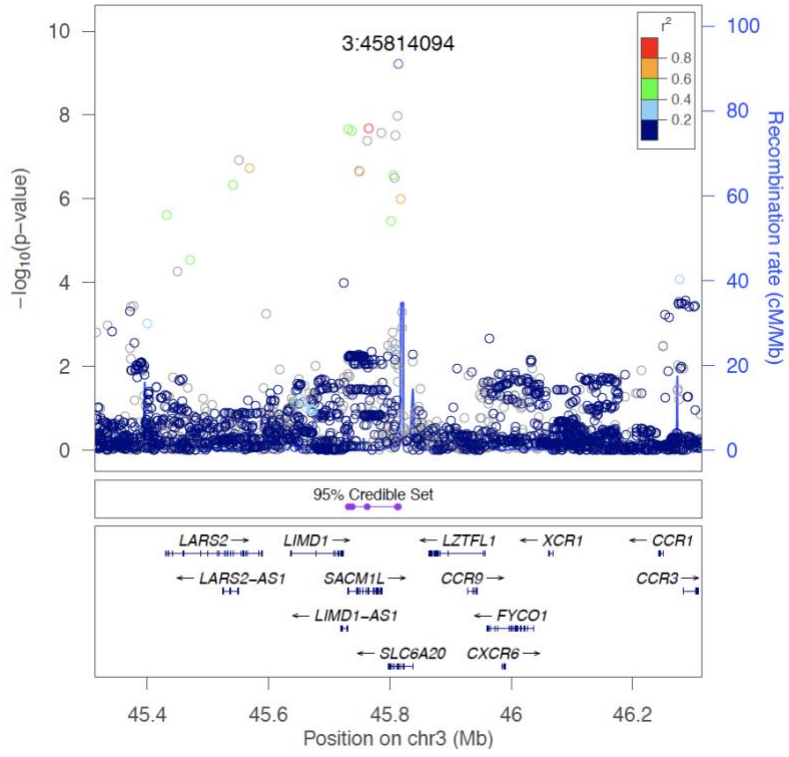
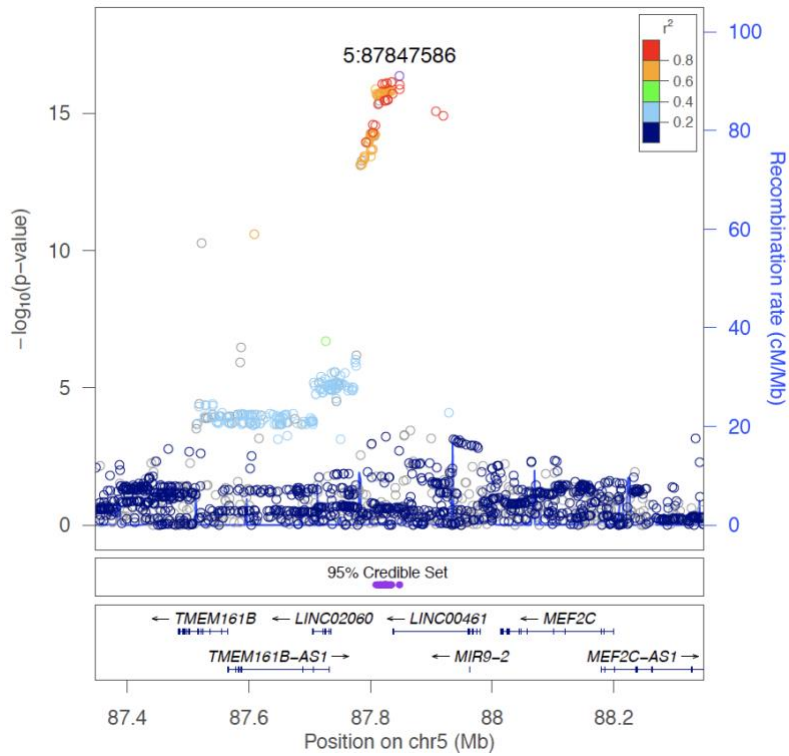
Figure S4. Quantile-quantile plots

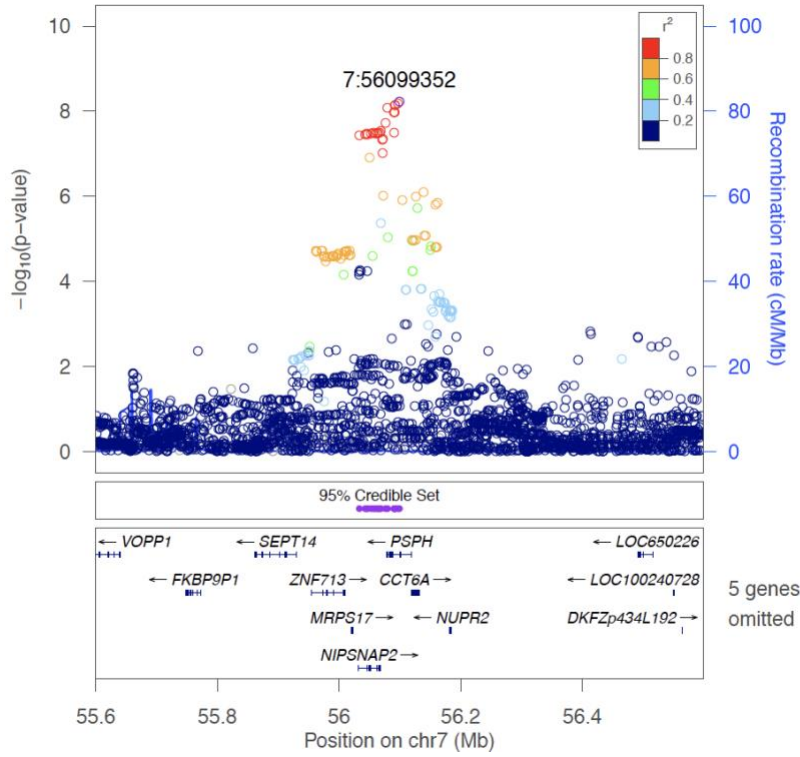
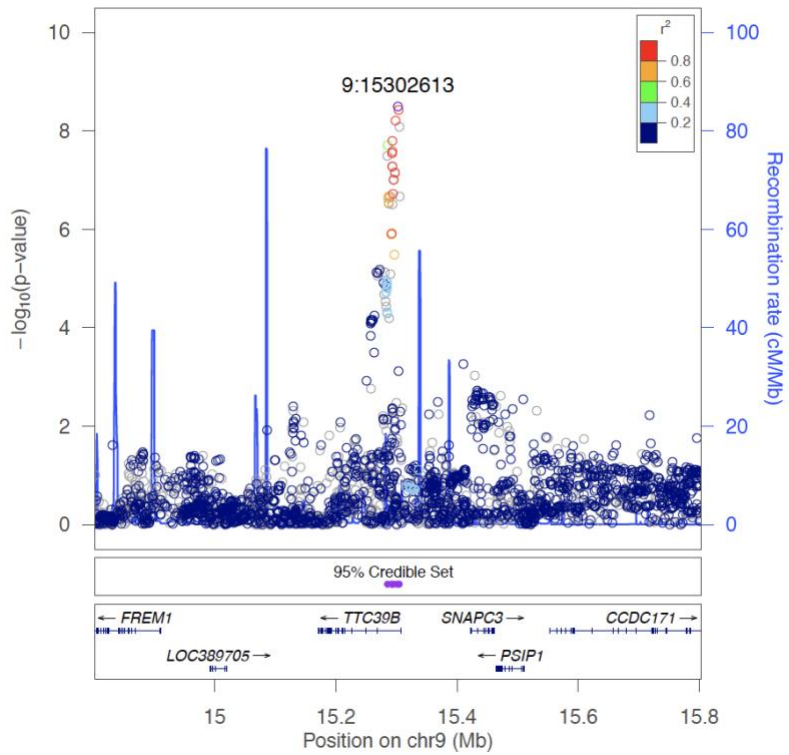
- A) All ancestry analysis - All SNPs (MAF $>$ 0.25% and INFO \geq 0.9) - $\lambda=1.011$
- B) European Ancestry only analysis - All SNPs (MAF $>$ 0.25% and INFO \geq 0.9) - $\lambda=1.013$
- C) All ancestry analysis - rare SNPs (MAF $<$ 5%), INFO \geq 0.9 - $\lambda=0.992$
- D) All ancestry analysis - common SNPs (MAF \geq 5%) and INFO \geq 0.9 - $\lambda=1.013$
- E) All ancestry analysis - rare SNPs (MAF $<$ 5%), INFO \geq 0.95 - $\lambda=0.991$
- F) All ancestry analysis - common SNPs (MAF \geq 5%) and INFO \geq 0.95 - $\lambda=1.014$
- G) European Ancestry analysis - rare SNPs (MAF $<$ 5%), INFO \geq 0.9 - $\lambda=0.983$
- H) European Ancestry analysis - common SNPs (MAF \geq 5%) and INFO \geq 0.9 - $\lambda=1.006$
- I) European Ancestry analysis - rare SNPs (MAF $<$ 5%), INFO \geq 0.95 - $\lambda=0.984$
- J) European Ancestry analysis - common SNPs (MAF \geq 5%) and INFO \geq 0.95 - $\lambda=1.009$

A**B**

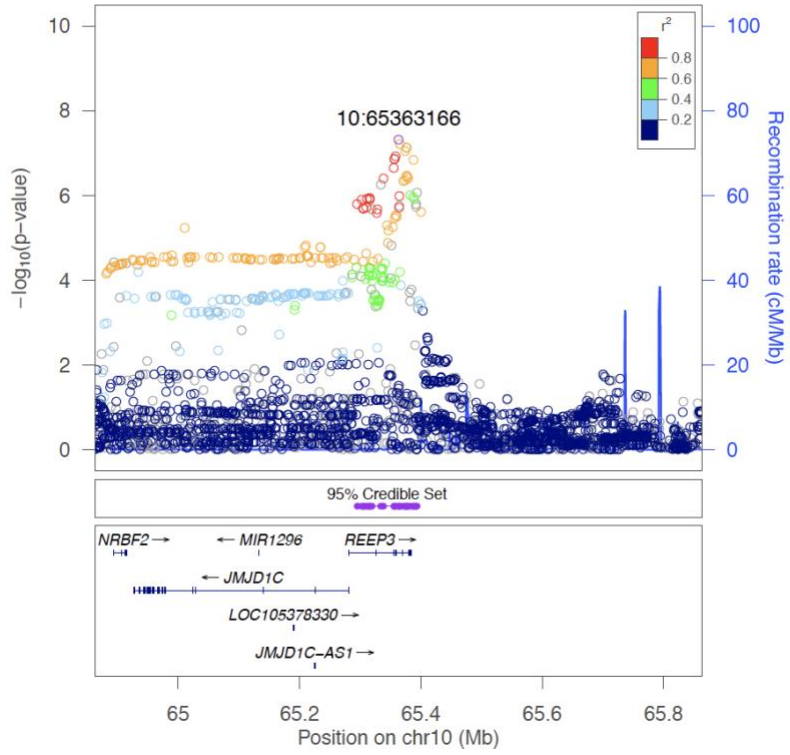
C**D**

E**F**

G**H**

I**J**

K



L

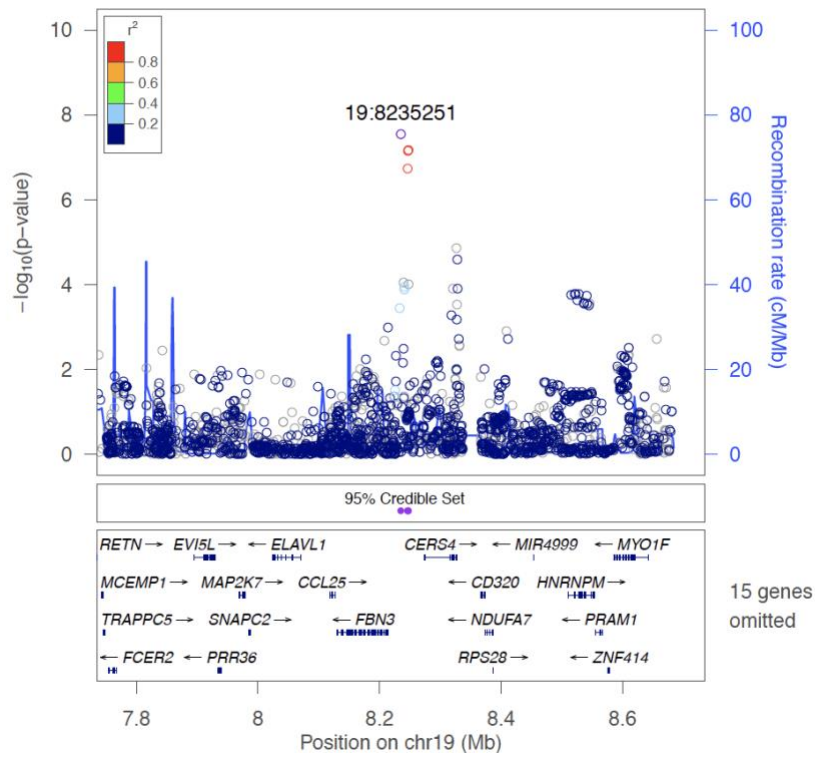


Figure S5. LocusZoom Plots for GW-significant loci including 95% CI for credible SNP set (purple bars). Gene boundaries are displayed by blue bars below plot.

A) 1p12 signal 1: Top SNP rs146953046 (chr1:120278072) - P-values conditional on rs146953046 (chr1:120265444).

B) 1p12 signal 2: Top SNP rs146953046 (chr1:120265444) - P-values conditional on rs146953046 (chr1:120278072).

C) 1p12 region with two independent signals: rs146953046 (chr1:120278072) and rs146953046 (chr1:120278072). Non-conditional P-values shown. SNPs in LD with rs146953046 (chr1:120278072) coloured in blue; SNPs in LD with rs146953046 (chr1:120265444) coloured in red.

D) 2p14 locus: Top SNP rs2160387 (chr2: 65220910).

E) 2q34 locus: Top SNP rs1047891 (chr2:211540507).

F) 3p24.1 locus: Top SNP rs9820465 (chr3:27706298).

G) 3p21.31locus: Top SNP rs17279437 (chr3:45814094).

H) 5q14.3 locus: Top SNP rs17421627 (chr5:87847586). I

) 7p11.2 locus: Top SNP rs6955423 (chr7:56099352).

J) 9p22.3 locus: Top SNP rs677622 (chr9:15302613).

K) 10q21.3 locus: Top SNP rs10995566 (chr10:65363166).

L) 19p13.2 locus: Top SNP rs139412173 (chr19:8235251).

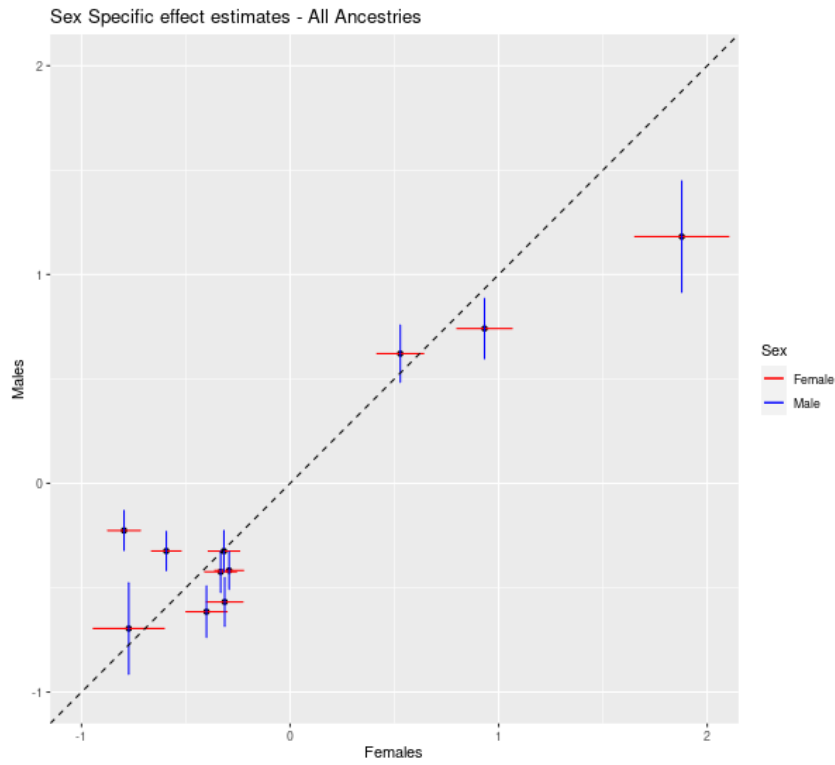
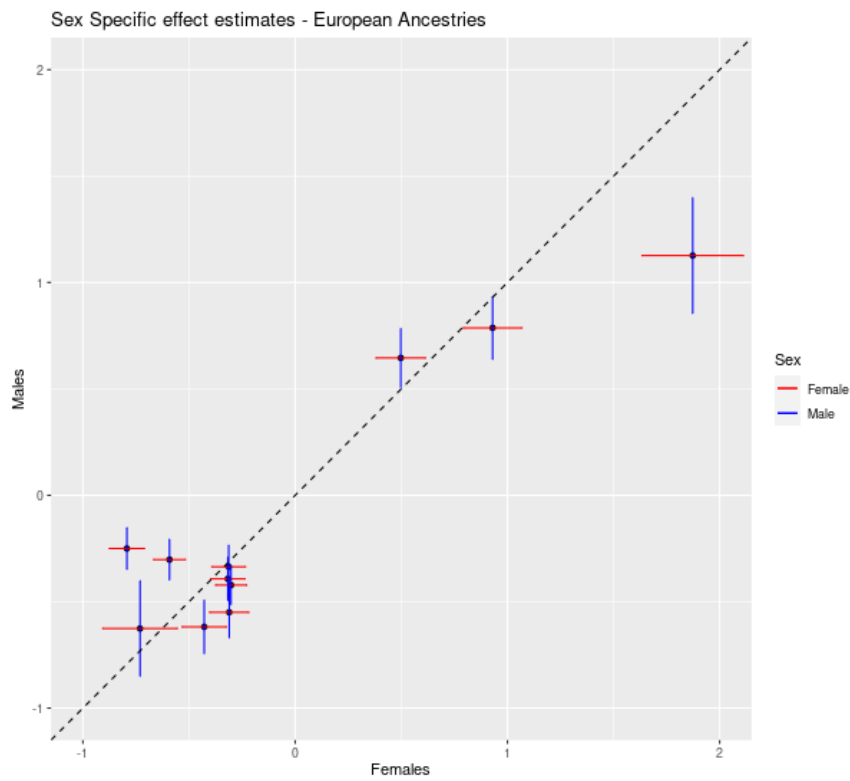
A**B**

Figure S6. Comparison of effect estimates (log odds ratios) in females (x-axis) and males (y-axis). Red and blue bars indicate standard errors of effect estimates. A) All ancestries analysis. B) European Ancestries analysis.

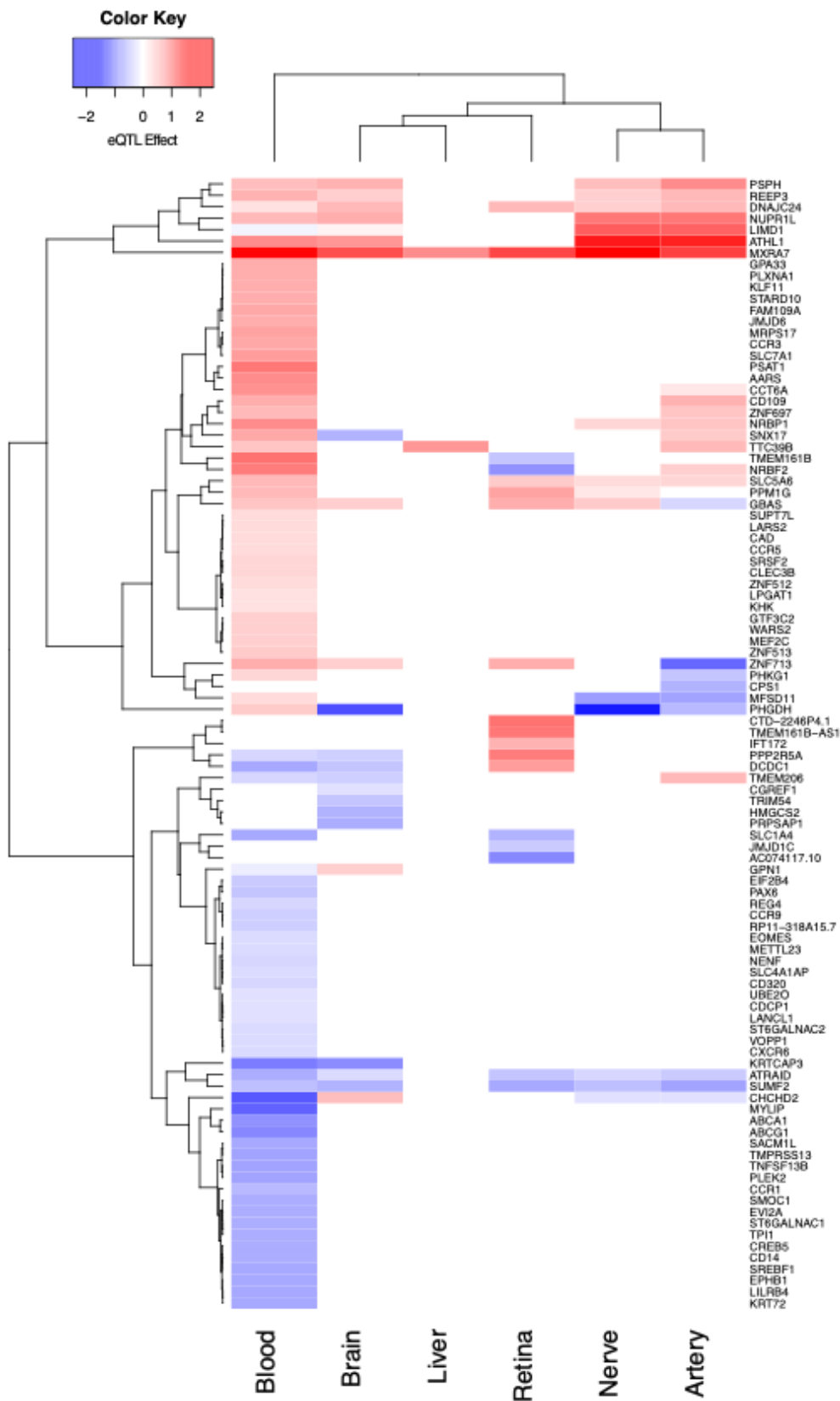


Figure S7. eQTL effects heatmap. The heatmap presents eQTL effects found across the analysed tissues. The average effect size of eQTL for each gene in each tissue is presented in the heatmap, non-significant eQTL are displayed in white. Genes and tissues are ordered according to hierarchical clustering modelling as presented in the image.

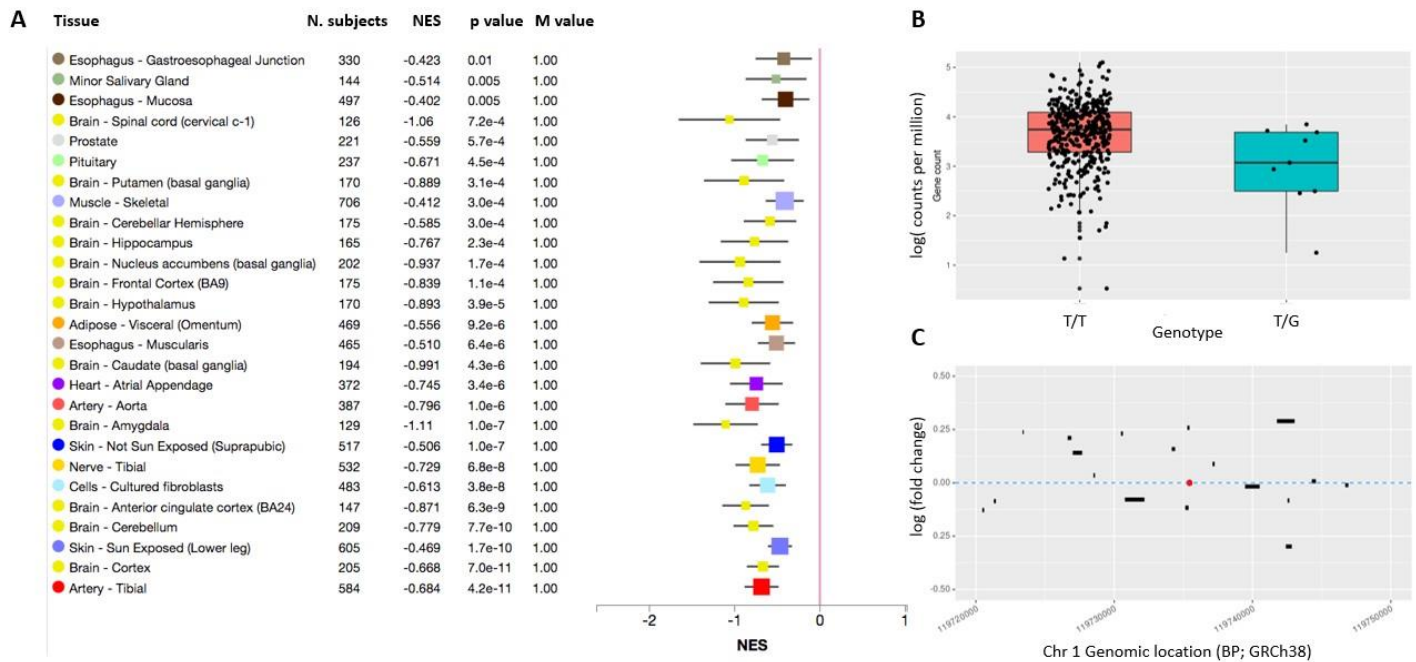


Figure S8. Effects of the rare deleterious SNP rs146953046 on gene expression and exon abundance in the GTEx database and the retina. A) Tissues in the GTEx database (y axis) for which the minor (G) allele of rs146953046 is associated with a significant difference in *PHGDH* gene expression with high confidence (M value =1). NES: normalized effect size (equivalent to alternative SNP beta value in a linear model); M value: posterior probability of eQTL. Horizontal whisker plots indicate the median (filled square) and 95% confidence interval (black bars) for NES estimates. In all tissues the effect of the G allele is suppressive. **B)** Expression of *PHGDH* in the retina (y axis; Ratnapriya *et al* 2019, *Nat Genet*) for individuals with the reference genotype (T/T) compared to heterozygotes (x axis). Each point represents *phgdh* expression measured in an individual donor retina. Box plot centre line: median; box limits: upper and lower quartiles; whiskers: 1.5x interquartile range. The difference between genotypes is significant ($p < 0.003$) after correcting for subject age, sex and AMD status. **C)** Relative expression of merged *PHGDH* exons in the neural retina between heterozygous individuals and reference homozygous individuals. The span of each exon across chromosome 1 (x axis) is indicated by black bars. The height of the exon bars relative to the y axis indicates log fold change. The red point indicates the genomic (intronic) location of the rare SNP.

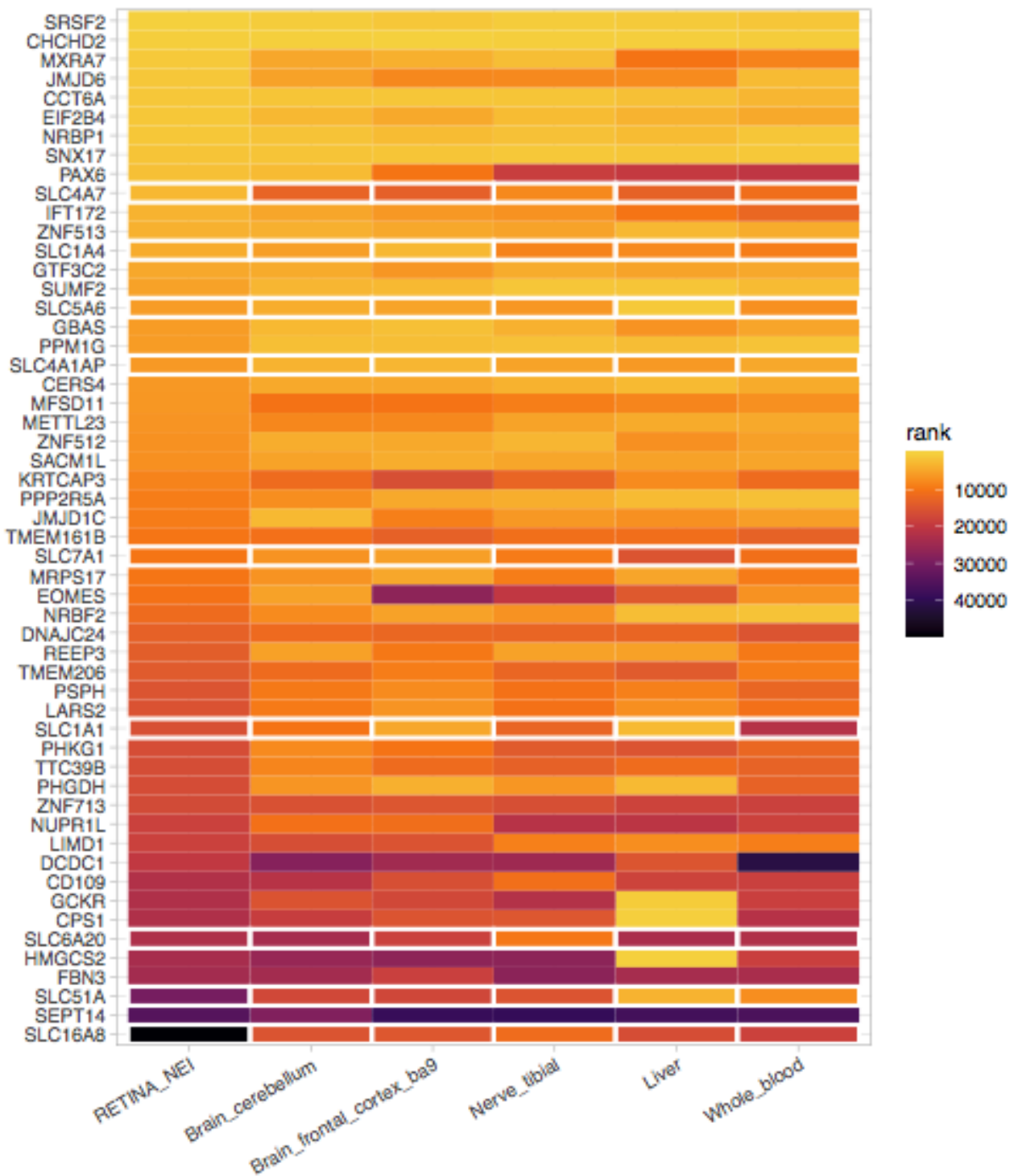


Figure S9. Ranked length-normalized gene expression (transcripts per million) for 55 genes prioritized in post-GWAS analyses, across multiple human tissues. Tiles outlined in white are solute-transport family genes. Tile color indicates transcriptional abundance rank within tissue (1 = highest expression rank = yellow). Median TPM for retina calculated based on gene expression data from 106 healthy retina donors, published by Ratnapriya et al. Expression for other tissues taken from GTEx supplementary data.

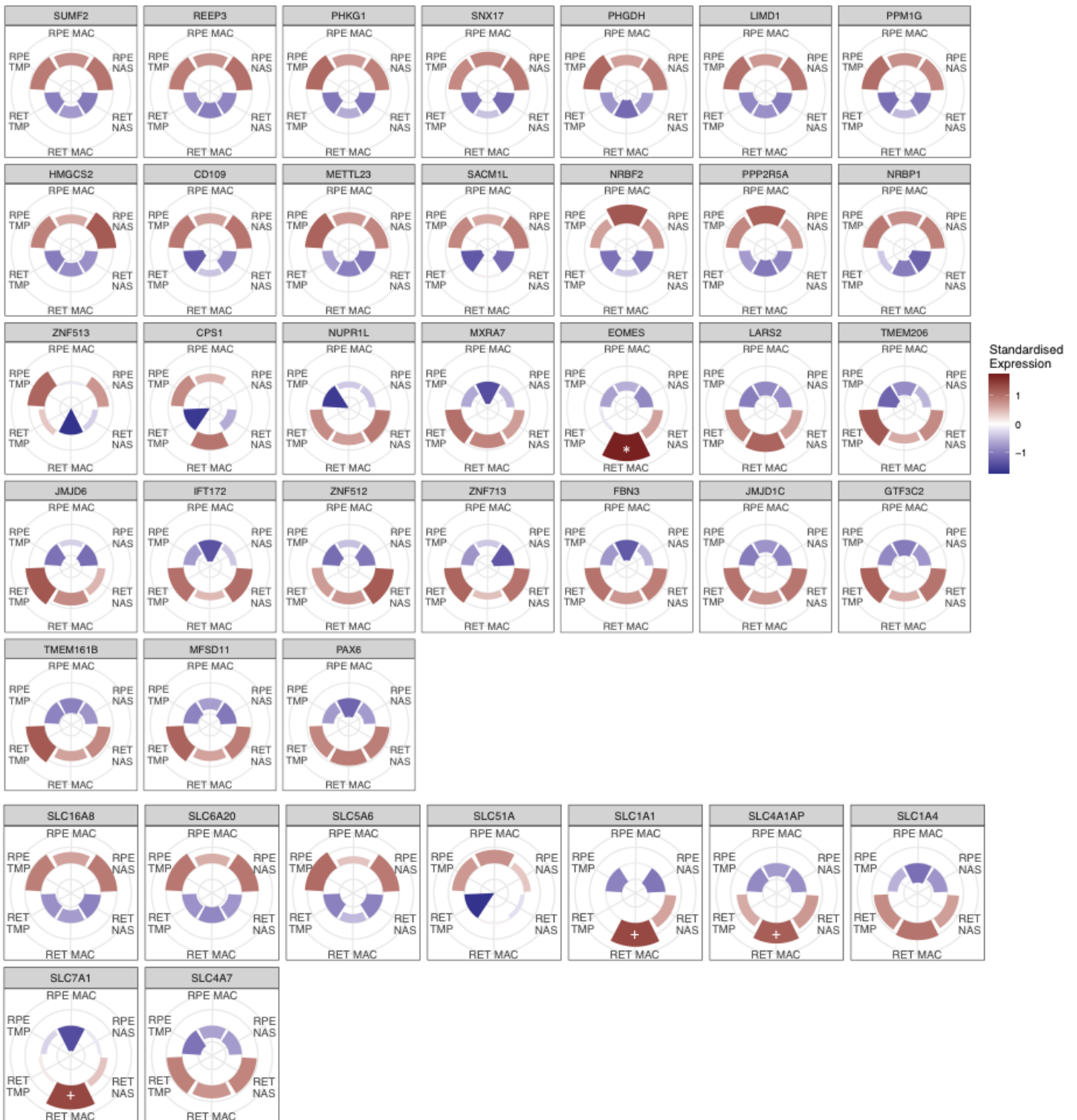


Figure S10. Relative expression patterns across retina (RET) and retinal pigment epithelium (RPE) for genes displaying significant differences between the two tissues, and between retinal regions. SLC family genes are grouped at the bottom (see also Table S12). TMP: temporal side; NAS: nasal side; MAC: macular region. NB SLC1A1 is not differentially abundant between RET and RPE, but shows area-specific enrichment. * enriched in MAC relative to NAS and TMP; + enriched in MAC relative to TMP.

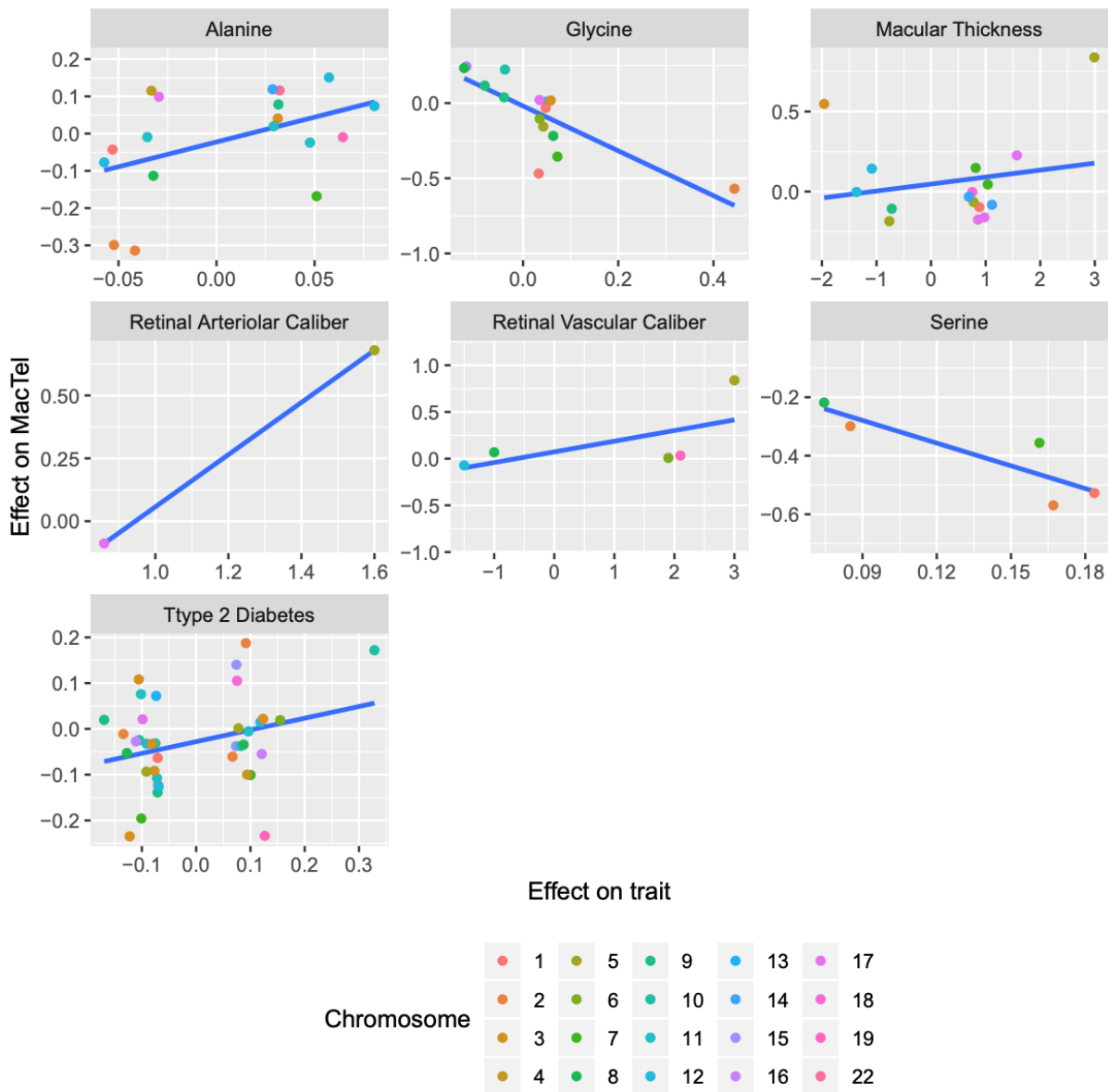


Figure S11. MacTel vs phenotype effect size comparison of SNPs instrument used in Mendelian Randomization. Each panel contains the effect size comparison for SNPs used in each phenotype. Each SNP is presented as a point, and different colours represent different chromosomes. X-axis presents the effect size on each phenotype of interest while y-axis presents the effect on MacTel disease.

Supplementary Note 1

Recruiting institutes and ethics approvals

The MacTel Project consortium recruited cases and controls at 24 participating clinical centers in seven countries (Australia, Germany, France, UK, Switzerland, Israel and United States). Informed written consent was obtained in accordance with ethics protocols for human subjects approved by the appropriate governing body at each site in accordance with the Declaration of Helsinki. Protocols and records of consent were centrally managed by the EMMES Corporation. The following ethics boards granted approval for human subject enrollment: Quinze-Vingts, Paris, France: Comité de Protection des Personnes Hôpital Saint-Antonie; Centre for Eye Research, Victoria, Australia: The Royal Victorian Eye and Ear Hospital; QIMR Berghofer Institute of Medical Research, Queensland, Australia; Clinique Ophtalmologie de Creteil, Paris, France: Comité de Protection des Personnes Hôpital Saint-Antonie; Hôpital Lariboisière, Paris, France: Comité de Protection des Personnes Hôpital Saint-Antonie; Jules Stein Eye Institute, UCLA, California, USA: The UCLA Institutional Review Board; Lions Eye Institute, Nedlands, Australia: Sire Charles Gairdner Group Human Research Ethics Committee; Manhattan Eye, Ear and Throat Hospital, New York, USA: Lenox Hill Hospital Institutional Review Board; Moorfields Eye Hospital, London, UK: National Research Ethics Service; Retina Associates of Cleveland, Inc., Cleveland, Ohio, USA: Sterling Institutional Review Board; Save Sight Institute, Sydney, Australia: South Eastern Sydney Illawarra Area Health Service Human Research Ethics Committee–Northern Hospital Network; Scripps Research Institute, La Jolla, California, USA: Scripps Institutional Review Board; St. Franziskus Hospital, Munster, Germany: Ethik-Kommission der Ärztekammer Westfalen-Lippe und der Medizinischen Fakultät der Westfälischen Wilhelms-Universität; The Goldschleger Eye Institute, Tel Hashomer, Israel: Ethics Committee The Chaim Sheba Medical Center; The New York Eye and Ear Infirmary, New York, USA: The Institutional Review Board of the New York Eye and Ear Infirmary; The Retina Group of Washington, Olympia, Washington, USA: Western Institutional Review Board; University of Bonn, Bonn, Germany: Rheinische Friedrich-Wilhelms-Universität Ethik-Kommission; University of Chicago, Chicago, Illinois, USA: The University of Chicago Division of Biological Sciences–The Pritzker School Institutional Review Board; University of Michigan, Ann Arbor, Michigan, USA: Medical School Institutional Review Board (IRBMED); University of Wisconsin, Madison, Wisconsin, USA: Office of Clinical Trials University of Wisconsin School of Medicine and Public Health; The Wilmer Eye Institute of Johns Hopkins University, Baltimore, Maryland, USA: Johns Hopkins School of Medicine Office of Human Subjects Research; Scheie Eye Institute University of Pennsylvania, Philadelphia, Pennsylvania, USA: University of Pennsylvania Office of Regulatory Affairs; University of Bern, Bern, Switzerland: Kantonale Ethikkommission Bern; John Moran Eye University of Utah, Salt Lake City, Utah, USA: The University of Utah Institutional Review Board; Bascom Palmer Eye Institute University of Miami, Miami, Florida, USA: The University of Miami Human Subjects Research Office; Columbia University, New York, New York, USA: Columbia University Medical Center Institutional Review Board Category 4 waiver for research involving specimens obtained from deidentified subjects.

Supplementary Methods

Patient Diagnosis

Protocol details of the multi-center Natural History Study of Macular Telangiectasia (MacTel Study) have been reported previously^{3,4}. The diagnosis of MacTel type 2 was based on characteristic morphologic findings on fundoscopy, optical coherence tomography (OCT), fundus fluorescein angiography (FFA) and fundus autofluorescence, and was confirmed by the Moorfields Eye Hospital Reading Centre, London, UK.

Sex Interaction analysis

For the top SNPs at each identified locus, we undertook analyses in males and females separately, with adjustment for 8 PCs of ancestry. In the all ancestries analyses, the females comprised of 644 cases and 2974 controls, and the males comprised of 423 cases and 825 controls. In the European ancestries analyses, the females comprised of 544 cases and 2941 controls, and the males comprised of 387 cases and 804 controls.

Given the unequal numbers of males and females, we formally tested for a sex interaction using Welsch's t-test:

$$t = \frac{\beta_F - \beta_M}{\sqrt{se_f^2 + se_M^2}}$$

With degrees of freedom:

$$d.f. = \frac{(se_F^2 + se_M^2)^2}{\frac{se_F^2}{n_f - 1} + \frac{se_M^2}{n_M - 1}}$$

P-values $< 4.5 \times 10^{-3}$ (Bonferroni correction for 11 SNPs), were considered significant evidence of a sex interaction.

Polygenic Risk Scores

We employed the software PRSice2²⁻⁴ to construct a third, even less stringent PRS comprising a much larger number of SNPs. Given the rarity of MacTel, we were not able to source an independent dataset to validate the prediction power of the PRS created by PRSice. In lieu of this, we tested the prediction model within the discovery dataset. We observed the PRS with the highest r^2 to contain 34,424 SNPs. This model was additionally different from the PRS with the lowest empirical p-value (613 SNPs) thus likely overfitting the model. For this reason and the lack of a truly independent validation set, we decided to discard the PRS estimated using PRSice.

Supplementary Note 2

Inflation of test statistics

QQ plots (Figure S4) and assessment of the genomic control inflation factors (λ_{GC}), indicated that population stratification was appropriately accounted for in both analyses (European analysis: $\lambda_{GC}=1.013$; full-cohort analysis: $\lambda_{GC}=1.011$). We additionally used LD score regression (LDSC) to assess confounding due to population stratification, however the LDSC intercepts were less than one in both analyses (European analysis: intercept = 0.974; full-cohort analysis: intercept = 0.975), likely due to the small sample size.

Mendelian Randomization

Consistent with the previously published results, we found type 2 diabetes PRS to be robustly associated with disease risk, this result remained significant even after inclusion of genetically-predicted serine, glycine and alanine in the model. MR-Egger test resulted non-significant for all three metabolites as well as T2D (b_0Ser P=0.76; b_0Gly P=0.86; b_0Ala P=0.40; b_0T2D P=0.73) discarding the hypothesis their association with MacTel risk arises from pleiotropic effects of the SNPs used to construct the PRS of these traits.

By comparing SNPs effect size between MacTel disease and the traits we tested for MR association we noticed that the relationship between retinal arteriolar calibre PRS, retinal vascular calibre PRS and retinal thickness PRS with MacTel disease was likely driven by single SNPs in locus 5q14.3 rather than a global effect (Figure S7). To this end, we included SNP rs17421627 in all three models as a covariate. Inclusion of this SNP resulted in retinal arteriolar calibre PRS ($b=-0.07$, $p=0.16$) and retinal vascular calibre PRS ($b=0.008$, $p=0.85$) to lose significance while macular thickness to change from a positive association to a negative association ($b=-0.088$, $p=0.046$). This last was again found to be entirely driven by SNP rs17279437 in locus 3p21.31 as the inclusion of this SNP resulted in a complete loss of significance between macular thickness and MacTel ($b=0.005$, $p=0.90$).

Supplementary References

1. Hutchinson, A., Watson, H. & Wallace, C. Improving the coverage of credible sets in Bayesian genetic fine-mapping. *PLoS Comput. Biol.* 16, e1007829 (2020).
2. Ratnapriya, R. *et al.* Retinal transcriptome and eQTL analyses identify genes associated with age-related macular degeneration. *Nat. Genet.* 51, 606–610 (2019).
3. Charbel Issa, P. *et al.* Macular telangiectasia type 2. *Prog. Retin. Eye Res.* 34, 49–77 (2013/5).
4. Clemons, T. E. *et al.* Baseline characteristics of participants in the natural history study of macular telangiectasia (MacTel) MacTel Project Report No. 2. *Ophthalmic Epidemiol.* 17, 66–73 (2010).